# Effect of hydrostatic pressure on the unconventional charge density wave and superconducting properties in two distinct phases of doped kagome superconductors CsV$_{3-x}$Ti$_x$Sb$_5$

J. Hou [1,2,*], K. Y. Chen,[1,2,*] J. P. Sun [1,2,†], Z. Zhao,[1,2] Y. H. Zhang,[1,2] P. F. Shan,[1,2] N. N. Wang,[1,2] H. Zhang,[1,2] K. Zhu,[1,2] Y. Uwatoko,[3] H. Chen,[1,2,4] H. T. Yang,[1,2,4,‡] X. L. Dong [1,2,4], H.-J. Gao,[1,2,4,5] and J.-G. Cheng [1,2]

[1]*Beijing National Laboratory for Condensed Matter Physics and Institute of Physics, Chinese Academy of Sciences, Beijing 100190, China*
[2]*School of Physical Sciences, University of Chinese Academy of Sciences, Beijing 100190, China*
[3]*Institute for Solid State Physics, University of Tokyo, Kashiwa, Chiba 277–8581, Japan*
[4]*Songshan Lake Materials Laboratory, Dongguan, Guangdong 523808, China*
[5]*CAS Center for Excellence in Topological Quantum Computation, University of Chinese Academy of Sciences, Beijing 100190, China*

Recent studies on the kagome metal CsV$_3$Sb$_5$ have revealed an intricate interplay between unconventional charge density waves (CDWs) and superconductivity (SC). Substitutions of Ti for V can perturb the CDW and produce two distinct SC phases with different pairing symmetries in the series of CsV$_{3-x}$Ti$_x$Sb$_5$. Here, we performed a comprehensive high-pressure study on Ti-doped CsV$_{3-x}$Ti$_x$Sb$_5$ ($x = 0.04$, 0.15) samples to elucidate the combined effects of physical pressure and chemical doping on the coexistence of CDWs and SC. Under high pressures, the M-shaped double superconducting dome observed in the parent CsV$_3$Sb$_5$ is retained but very weakened for $x = 0.04$, and it is replaced by a single broad superconducting dome for $x = 0.15$. Accordingly, the optimal superconducting $T_c$ under high pressures decreases gradually with increasing Ti-doping level. On the other hand, the upper critical field first exhibits an obvious rise with enhanced flux pinning effects by disorders for $x = 0.04$ and then is suppressed upon further increasing Ti doping. The constructed $T$-$P$ phase diagrams of CsV$_{3-x}$Ti$_x$Sb$_5$ reveal the competition and coexistence of CDWs and SC. Our results provide more insight into the intertwined competing electronic orders in the Ti-doped kagome superconductors CsV$_{3-x}$Ti$_x$Sb$_5$.

## I. INTRODUCTION

Recently, the family of kagome metals $A$V$_3$Sb$_5$ ($A =$ K, Rb, or Cs) has emerged as a material platform for the experimental realizations of theoretically predicted quantum states of the kagome lattice model [1–5], including the nontrivial band topology, charge density waves (CDWs), and superconductivity (SC) [6–11]. At ambient pressure (AP), CsV$_3$Sb$_5$ undergoes three consecutive phase transitions upon cooling down; it first forms a three-dimensional triple-$Q_{2a0}$ CDW below $T_{CDW} \approx 94$ K [6,12–14], followed by the emergence of an electronic nematicity at $T_{nem} \approx 35$ K [15], and then enters the superconducting state below $T_c \approx 2.5$ K [6]. Under high pressures, $T_{CDW}$ is monotonically suppressed by $\sim$2 GPa, while $T_c(P)$ exhibits an unusual M-shaped double superconducting dome with the two extremes occurring at the exact pressures where the CDW experiences subtle modifications and vanishes [16,17], respectively. Subsequent experimental investigations have indeed revealed an intricate interplay between CDWs and SC in CsV$_3$Sb$_5$ [18,19]. According to high-pressure nuclear magnetic resonance (NMR) experiments, the change of resistivity anomaly at $T_{CDW}$ is correlated with a transition of the CDW from triple-$Q_{2a0}$ to stripe-type

at the critical pressure of $P_{c1}$ [19]. Therefore, the observed broadened superconducting transition width in between $P_{c1}$ and $P_{c2}$ should originate from the strong competition between stripe-type CDWs and SC. On the other hand, with reducing the $A$-cation size or the interlayer distance, the double dome of the superconducting phase for $A =$ Cs is gradually weakened for $A =$ Rb and finally changed to a single dome for $A =$ K under high pressures [16,17,20,21]. Uniaxial strain experiments further confirmed that the interlayer distance plays an important role in producing such an unusual phase diagram [22], which is also indicated by density functional theory (DFT) calculations [16,23,24]. It remains unclear whether the stripe-type CDW is gradually suppressed or even disappears based on the shape of the superconducting phase with the reduction of $A$-cation size from Cs to K. More experiments are needed to unveil the intricate interplay between CDWs and SC in this family of kagome superconductors.

In addition to high pressure, chemical doping is another effective means to tune the coexistence and competition between CDWs and SC through introducing disorders or altering the chemical potential. Recently, several groups have studied the effects of Ti- and Nb-doping at the V sites and Sn-doping at the Sb sites of bulk CsV$_3$Sb$_5$ [25–28]. Hole doping in the series of CsV$_{3-x}$Ti$_x$Sb$_5$ [27,28] and CsV$_3$Sb$_{5-x}$Sn$_x$ [26] lowers the chemical potential, pushes the van Hove singularity (vHS) gradually above the Fermi level, and leads to a quick suppression of the CDW. This indicates that the CDW of CsV$_3$Sb$_5$ has direct correlation with the vHS. Moreover, the

*These authors contributed equally to this work.

†jpsun@iphy.ac.cn

‡htyang@iphy.ac.cn

superconducting phase exhibits an M-shaped double-dome structure [26,27]. However, the isovalent substitutions of Nb for V merely induce a monotonic enhancement of superconducting transition with the concomitant suppression of the CDW [25]. Angle-resolved photoemission spectroscopy (ARPES) measurements and first-principles simulations confirm the direct correlation between CDWs and the vHS, while SC may not be associated with CDWs [28]. Considering that there still exist controversial issues on the correlation between CDWs and SC in these doped $CsV_3Sb_5$, it is necessary to investigate the pressure effect on these doped samples for further clarifying and understanding the relationship between unconventional CDWs and SC.

Here, we have chosen Ti-doped $CsV_{3-x}Ti_xSb_5$ as the target system because it exhibits two distinct superconducting phases with different pairing symmetry [27]. Through detailed resistivity and magnetic susceptibility measurements on $CsV_{3-x}Ti_xSb_5$ ($x = 0.04$ and 0.15) single crystals, we reveal an obvious modification of the M-shaped superconducting dome at $P_{c1}$ for $x = 0.04$ and a single superconducting dome for $x = 0.15$. The maximum $T_c$ under pressure also decreases with increasing Ti dopants from $x = 0$ to 0.15. The constructed $T$-$P$ phase diagram of $CsV_{2.96}Ti_{0.04}Sb_5$ indicates the competition and coexistent nature between CDWs and SC, while the dome-shaped superconducting phase for $CsV_{2.85}Ti_{0.15}Sb_5$ may be correlated with the suppression of short-range CDWs. Moreover, the optimal upper critical field for $x = 0.04$ under high pressure shows an obvious increase, which should be attributed to the enhanced flux pinning effects by introducing Ti dopants. These results shed more light on understanding the intertwined competing electronic orders in this family of kagome superconductors.

## II. EXPERIMENTAL DETAILS

Single crystals of $CsV_{3-x}Ti_xSb_5$ were grown by using the self-flux method. Details about the crystal growth and characterizations at AP can be found in Ref. [27]. The structure and chemical composition of the samples used in this high-pressure study were characterized by x-ray diffraction (XRD) and energy dispersive spectroscopy, respectively, as shown in Figs. S1 and S2 in the Supplemental Material (SM) [29]. Temperature dependences of resistivity for $CsV_{3-x}Ti_xSb_5$ samples with $x = 0.04$ and 0.15 and ac magnetic susceptibility for $x = 0.15$ were measured simultaneously by using a self-clamped piston cylinder cell (PCC) under various hydrostatic pressures up to 2.19 GPa. Daphne 7373 was employed as the pressure-transmitting medium. Here, we use the standard four-probe method for resistivity measurements with the electrical current applied within the *ab* plane of single crystals. The magnetic field was applied along the *c* axis. For the ac susceptibility measurements, a piece of Pb was placed in the same coil with the sample by using the mutual induction method. The superconducting transition of Pb was used to determine the pressure values in PCC according to the equation $P(GPa) = (T_0 - T_c)/0.365$, where $T_0 = 7.20$ K is the $T_c$ of Pb at AP. In addition, the diamagnetic response of Pb can be used to estimate the superconducting shielding volume of the sample.

## III. RESULTS AND DISCUSSION

Figure 1 shows the temperature dependence of in-plane resistivity $\rho(T)$ of $CsV_{3-x}Ti_xSb_5$ ($x = 0$, 0.04, and 0.15) single crystals at AP. As shown in Fig. 1(a), the normal-state $\rho(T)$ displays the typical metallic behavior for these three samples, while the residual resistivity ratio = $\rho(290$ K$)/\rho(5$ K$)$ gradually decreases with increasing the Ti-doping level. This indicates that the chemical disorders introduced by Ti doping have a strong impact on the transport properties. Moreover, the kinklike anomaly in $\rho(T)$ associated with the formation of CDW order can be clearly observed at $T^* \approx 94$ K for $x = 0$ and $T^* \approx 80$ K for $x = 0.04$, as indicated by the red arrows in resistivity, Fig. 1(a), and the corresponding peaks in $d\rho/dT$, Fig. 1(b). Such an anomaly cannot be discerned anymore for the $x = 0.15$ sample, indicating the suppression of long-range CDW order. The enlarged view of $\rho(T)$ at $T < 5$ K, as shown in Fig. 1(c), depicts the superconducting transitions, which starts at $T_c^{onset} \approx 3.8$ K and reaches zero resistance at $T_c^{zero} \approx 2.8$ K for $x = 0$. Here, the $T_c^{onset}$ is determined as the temperature where $\rho(T)$ starts to deviate from the normal-state behavior, and $T_c^{zero}$ is defined as the zero-resistivity temperature. Upon Ti doping, the values of $T_c^{onset}$ and $T_c^{zero}$ first decrease to 2.9 and 1.65 K for $x = 0.04$ and then are enhanced to $\sim$4 and 2.4 K for $x = 0.15$. The nonmonotonic variation of $T_c(P)$ accompanying the monotonic suppression of $T^*$ as a function of Ti doping is summarized in the $T$-$x$ phase diagram of Fig. 1(d), consistent with the appearance of two distinct superconducting domes. All these results are in good agreement with a previous report [27].

Then we performed high-pressure transport measurements on the $x = 0.04$ and 0.15 single-crystal samples in PCC under various pressures up to 2.19 GPa. Figures 2(a) and 2(c) display the temperature dependences of $\rho(T)$ at $T < 100$ K for these two samples, and Fig. 2(b) shows the derivative $d\rho/dT$ at $T < 100$ K for $x = 0.04$. Here, both $\rho(T)$ and $d\rho/dT$ data were vertically shifted for clarity. The resistivity data in the whole temperature range are given in Fig. S3 in the SM [29]. At AP, the kinklike anomaly at $T^*$ in $\rho(T)$ and the corresponding peak in $d\rho/dT$ can be seen clearly in Figs. 2(a) and 2(b). When the pressure increases gradually, $T^*$ continuously shifts to lower temperatures and cannot be distinguished at $P > 1.5$ GPa, implying a complete suppression of CDW by pressure. It should be noted that the CDW-related anomaly gradually changes from a kinklike to a humplike anomaly in $\rho(T)$ and from a peak to a dip in $d\rho/dT$ at $P > 0.8$ GPa, which is like the results of $CsV_3Sb_5$ and $RbV_3Sb_5$ under high pressure, indicating the presence of similar pressure-induced modification of the CDW [16,21]. According to the recent high-pressure NMR and XRD experiments, the separation of a conjoined CDW and a transition from triple-$Q_{2a0}$ to a stripe-type CDW at the critical pressure $P_{c1}$ can explain this subtle modification of the CDW in $\rho(T)$ and $d\rho/dT$ [18,19]. For $CsV_{2.85}Ti_{0.15}Sb_5$ without a CDW at AP, the $\rho(T)$ shows a continuous and smooth decrease with increasing pressure to 2.19 GPa, as displayed in Fig. 2(c).

Figures 3(a) and 3(b), 3(c) show the enlarged view of low-temperature resistivity $\rho(T)$ and magnetic susceptibility $\chi'(T)$ curves for $CsV_{2.96}Ti_{0.04}Sb_5$ and $CsV_{2.85}Ti_{0.15}Sb_5$ samples, respectively. The superconducting transition
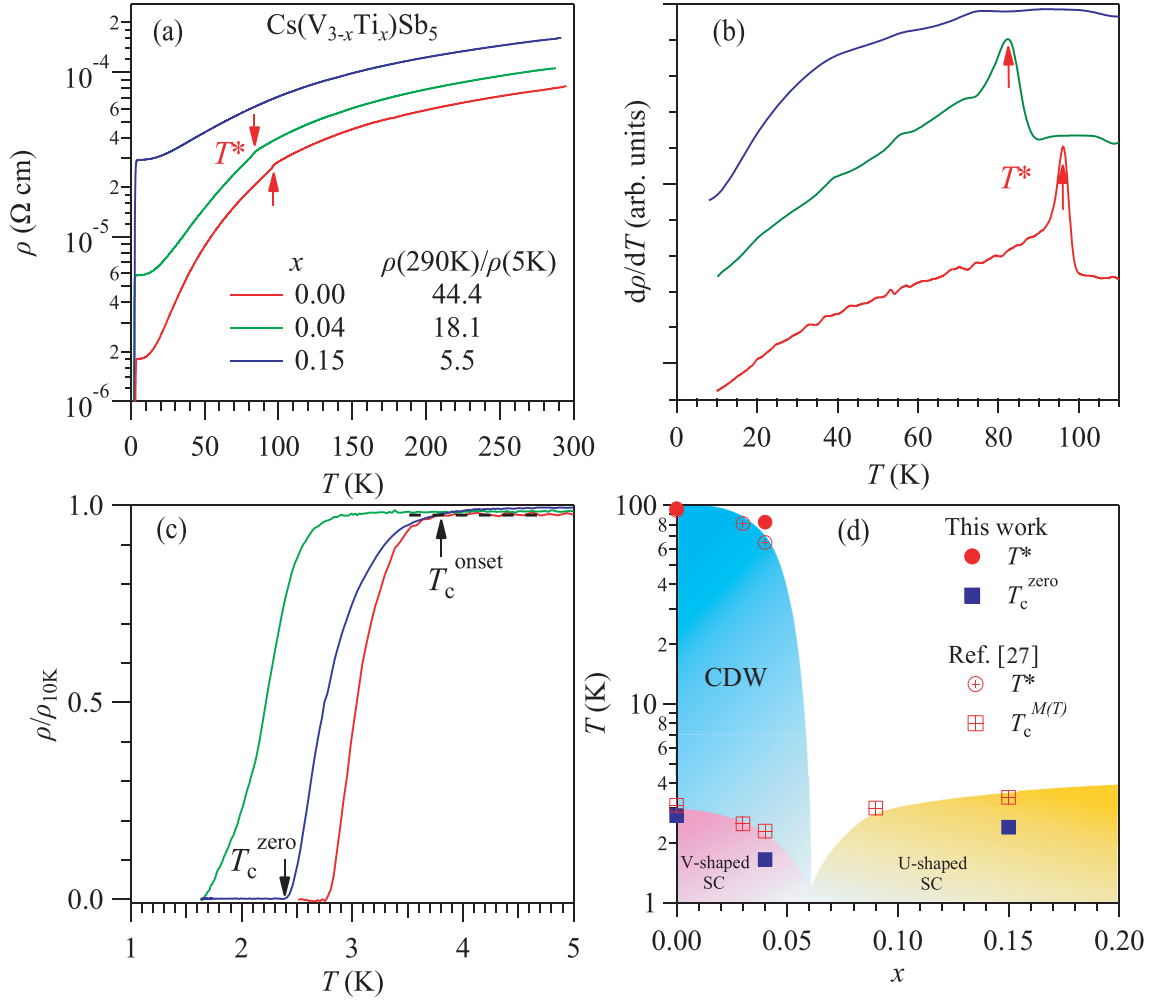
FIG. 1. (a) Temperature dependence of resistivity $\rho(T)$ for the series of $Cs(V_{3-x}Ti_x)Sb_5$ samples ($x = 0$, 0.04, and 0.15). (b) The corresponding $d\rho/dT$ curves at $T < 110$ K. (c) The resistivity curves at $T < 5$ K normalized to the values at 10 K for the three samples. (d) The phase diagram of $Cs(V_{1-x}Ti_x)_3Sb_5$, which illustrates the correlation between CDWs and SC. The transition temperatures of CDWs and SC are marked by the red and black arrows in the figures.

temperatures $T_c^{onset}$ and $T_c^{zero}$ are determined from $\rho(T)$ by using the same criteria as seen in Fig. 1(c), while for magnetic susceptibility, the $T_c^{\chi'}$ was defined as the intersection of two straight lines above and below the superconducting transition. As displayed in Fig. 3, the nonmonotonic evolution of $T_c$ under high pressure can be seen clearly for both samples. For $CsV_{2.96}Ti_{0.04}Sb_5$, we have extracted $T_c^{onset} \approx 2.9$ K and $T_c^{zero} \approx 1.65$ K at AP, leading to a $\Delta T_c = T_c^{onset} - T_c^{zero} \approx 1.25$ K. When we gradually increase the pressure, $T_c^{zero}$ first exhibits a sharp increase to ~3.5 K at 0.67 GPa and then shows a saturation around 1.2 GPa. Interestingly, the superconducting transition width $\Delta T_c$ displays a rapid increase in this pressure range, and it should correlate with the modification of the CDW, as discussed in Figs. 2(a) and 2(b). With further increasing pressure to 1.66 GPa, the superconducting transition shows a sudden increase to $T_c^{onset} \approx 7.9$ K and $T_c^{zero} \approx 7.65$ K, giving rise to a quite narrow $\Delta T_c \approx 0.25$ K at this pressure accompanied with a complete suppression of the CDW. Above 1.66 GPa, both $T_c^{onset}$ and $T_c^{zero}$ move down progressively, and $\Delta T_c$ remains nearly unchanged.

For $CsV_{2.85}Ti_{0.15}Sb_5$ without a CDW, the superconducting transition is quite broad with $T_c^{onset} \approx 3.8$ K and $T_c^{zero} \approx 2.4$ K at AP, as shown in Fig. 3(b). With increasing pressure gradually, both $T_c^{onset}$ and $T_c^{zero}$ exhibit an obvious increase, and $\Delta T_c$ narrows down progressively at $P < 1.5$ GPa. At 1.5 GPa, the superconducting transition is very sharp, and $T_c^{onset}$ and $T_c^{zero}$ reach the optimal values ~6.3 and ~6.1 K with $\Delta T_c \approx 0.2$ K. When the pressure is further increased to 2.19 GPa, the superconducting transition is suppressed to $T_c^{onset} \approx 5.7$ K and $T_c^{zero} \approx 5.5$ K, leaving $\Delta T_c$ almost unchanged. Here, we also measured the ac susceptibility $\chi'(T)$ to further verify the superconducting transitions of $CsV_{2.85}Ti_{0.15}Sb_5$, Fig. 3(c), in which the superconducting diamagnetic signal appears below $T_c^{\chi'}$, as indicated by the arrows. The obtained $T_c^{\chi'}$ first increases with pressure, reaches the maximum value near $P_c \approx 1.5$ GPa, and then decreases gradually upon further increasing pressure to 2.19 GPa. All the susceptibility data are in good agreement with the resistivity data. In addition, the superconducting shielding volume fraction can be
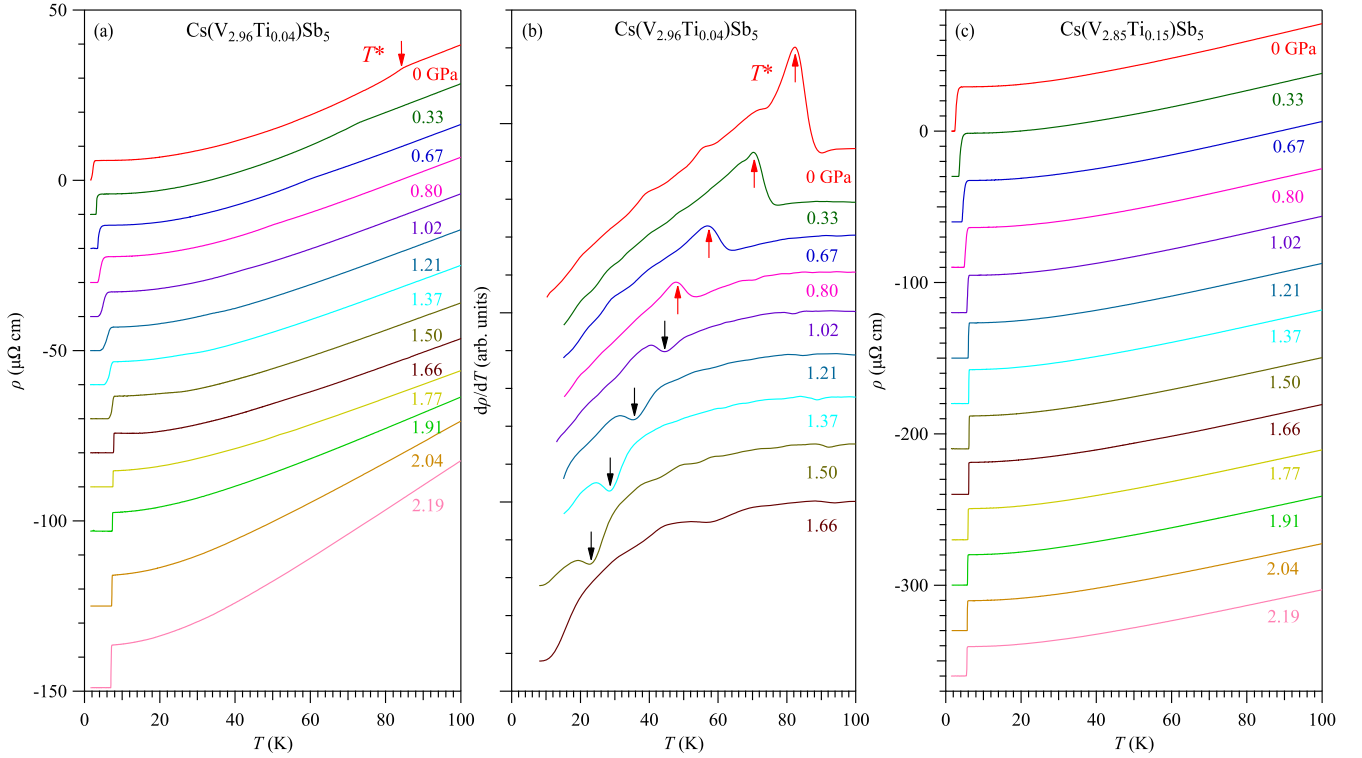
FIG. 2. Temperature dependences of (a) resistivity $\rho(T)$ and (b) its derivative $d\rho/dT$ for Cs(V$_{2.96}$Ti$_{0.04}$)Sb$_5$ and (c) resistivity $\rho(T)$ for Cs(V$_{2.85}$Ti$_{0.15}$)Sb$_5$ measured in a piston cylinder cell (PCC) under various pressures up to 2.19 GPa. The CDW ordering temperature $T^*$ is marked by the arrows in the figures. All the curves except that at 0 GPa have been shifted vertically for clarity.
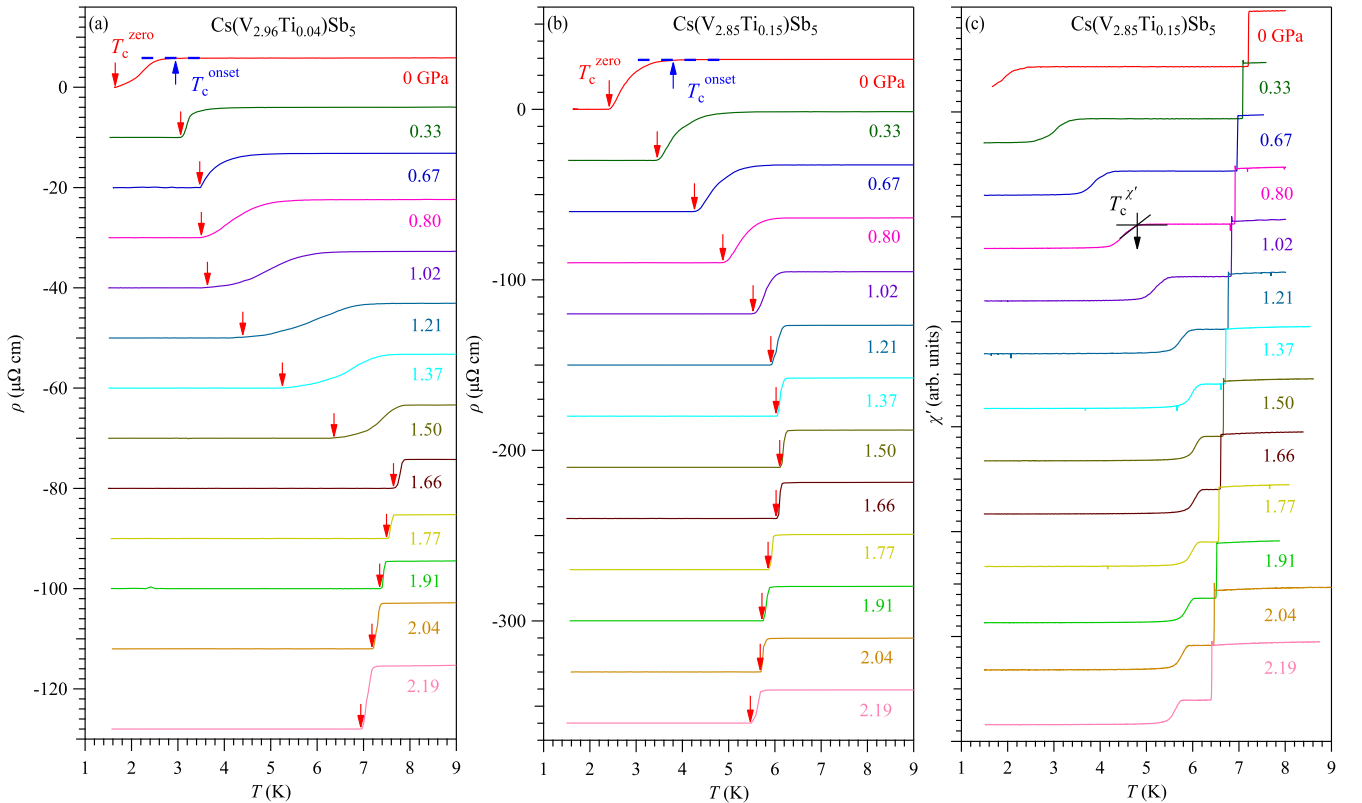


FIG. 3. Temperature dependences of (a) and (b) resistivity and (c) ac magnetic susceptibility of Cs(V$_{0.96}$Ti$_{0.04}$)Sb$_5$ and Cs(V$_{2.85}$Ti$_{0.15}$)Sb$_5$ at low-temperature range for tracking the superconducting transition under high pressures up to 2.19 GPa. All the curves except that at 0 GPa have been shifted vertically for clarity.
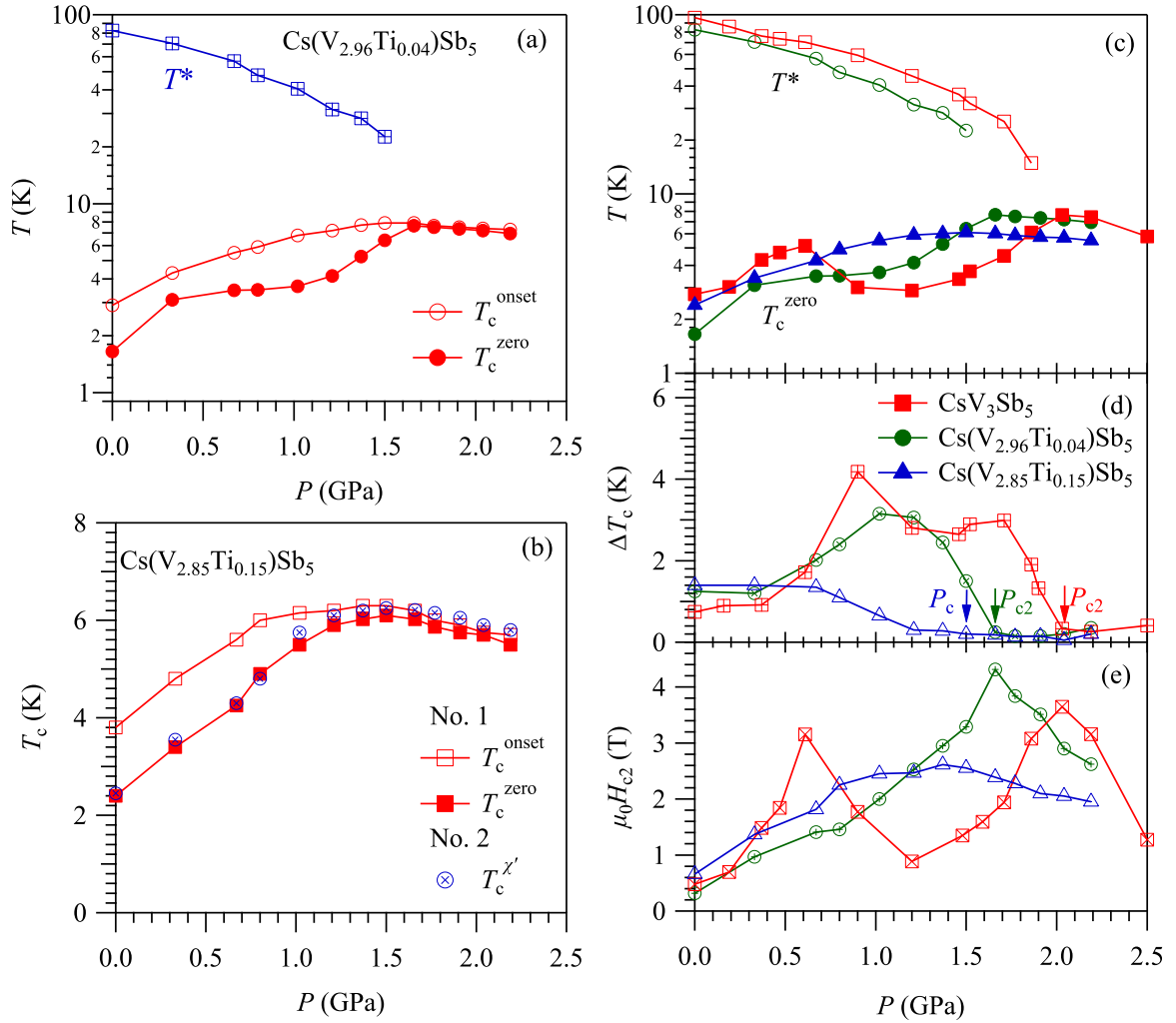
FIG. 4. Temperature-pressure phase diagram of $Cs(V_{3-x}Ti_x)Sb_5$ ($x = 0$, 0.04, and 0.15). Pressure dependences of $T^*$, $T_c^{onset}$, $T_c^{zero}$, and $T_c^{\chi'}$ for (a) $Cs(V_{0.96}Ti_{0.04})Sb_5$ in logarithmic scale and (b) $Cs(V_{2.85}Ti_{0.15})Sb_5$. (c) $T^*$ and $T_c^{zero}$ in logarithmic scale, (d) the superconducting transition width $\Delta T_c$ determined from the resistivity, and (e) the zero-temperature upper critical field $\mu_0 H_{c2}(0)$ obtained from the empirical Ginzburg-Landau (GL) fitting as a function of pressure for $Cs(V_{3-x}Ti_x)Sb_5$ ($x = 0$, 0.04, and 0.15).

estimated as ∼90% at each pressure by comparing with the diamagnetic response of Pb, thus confirming the bulk nature of the observed SC.

Based on the above high-pressure resistivity and magnetic susceptibility characterizations, the comprehensive temperature-pressure ($T$-$P$) phase diagrams were constructed for $CsV_{2.96}Ti_{0.04}Sb_5$ and $CsV_{2.85}Ti_{0.15}Sb_5$, as displayed in Figs. 4(a) and 4(b). To obtain a systematic understanding of the pressure effects on the series of Ti-doped kagome superconductors $CsV_{3-x}Ti_xSb_5$, we added our previous high-pressure results on $CsV_3Sb_5$ to the phase diagram, Fig. 4(c). From Figs. 4(a)–4(c), the detailed evolutions and intricate interplay between CDWs and SC are easily visualized as a function of hole doping, disorders, and high pressure. Although the CDW was suppressed to a lower temperature with Ti doping from $x = 0$ to 0.04, the superconducting $T_c$ shows a small decrease at the same time, implying that some factors brought by slight Ti doping are detrimental to both CDWs and SC at AP. Under high pressure, the CDW ordering temperature is suppressed monotonically, and the superconducting $T_c^{onset}$ shows a single domed structure optimized at

∼1.66 GPa, while $T_c^{zero}$ exhibits an intricate evolution. First, $T_c^{zero}$ increases rapidly at $P < 0.7$ GPa and shows a plateau with a corresponding modification of the CDW between 0.7 and 1.2 GPa. Furthermore, it displays a dramatic enhancement to the optimal value at ∼1.66 GPa by completely suppressing the CDW and then decreases again at $P > 1.66$ GPa. These results indicate that an intimate correlation and strong competing nature exist between CDWs and SC. The optimal $T_c^{onset} \approx 7.9$ K is achieved at around $P_{c2}$, and it is slightly lower than that in the parent $CsV_3Sb_5$, presumably due to the introduction of disorders.

For $CsV_{2.85}Ti_{0.15}Sb_5$ with a higher Ti-doping level, the long-range CDW has already been suppressed completely, and $T_c^{onset}$ and $T_c^{zero}$ were further enhanced to ∼3.8 and ∼2.4 K at AP, Fig. 1(b). As seen in Fig. 4(b), both $T_c^{onset}$ and $T_c^{zero}$ move up progressively to the maximum of ∼6.3 and ∼6.1 K at 1.5 GPa, above which the superconducting transition becomes sharper with $\Delta T_c \approx 0.2$ K. With further increasing pressure to 2.19 GPa, $T_c$ was suppressed gradually with very sharp transition $\Delta T_c \approx 0.15$ K. Interestingly, $T_c^{\chi'}$ agrees well with $T_c^{zero}$ at $P < 1.5$ GPa, where the superconducting transition is

broad, as commonly seen in most superconductors, whereas $T_c^{\chi'}$ follows $T_c^{\text{onset}}$ at $P > 1.5$ GPa, indicating that a considerable superconducting phase already appears near $T_c^{\text{onset}}$.

To obtain more information of the electronic states, we performed the resistivity measurements under magnetic fields at various pressures up to 2.19 GPa in both samples, as shown in Figs. S4 and S5 in the SM [29]. As we can see, a two-steplike superconducting transition emerges at $P > 1.5$ GPa for $x = 0.04$ and at a relative low pressure for $x = 0.15$ under high magnetic fields. Considering the disorders or defects introduced by Ti doping, it is expected that the magnetic flux pinning effects will be enhanced accompanying the increase of the chemical doping level. Therefore, the two-steplike superconducting transition should originate from flux pinning effects induced by the Ti dopants. Here, we use the middle-point temperature $T_c^{\text{mid}}$ as the superconducting transition temperature and employ the empirical Ginzburg-Landau fitting to extract the zero-temperature upper critical field $\mu_0 H_{c2}(0)$ at different pressures. As shown in Fig. 4(e), $\mu_0 H_{c2}(0)$ first exhibits a plateau between 0.5 and 1 GPa with a modification of the CDW and then shows a sharp peak at $\sim$1.66 GPa, where the CDW was completely suppressed for $CsV_{2.96}Ti_{0.04}Sb_5$. While for $CsV_{2.85}Ti_{0.15}Sb_5$, the broad dome-shaped $\mu_0 H_{c2}(0)$ can be seen clearly. Interestingly, the pronounced $\mu_0 H_{c2}(0)$ peaks are correlated with a modification or a quantum critical point (QCP) of the CDW and have a direct correlation with the superconducting transition width. Moreover, the corresponding optimal $\mu_0 H_{c2}(0)$ at $P_{c2}$ for $CsV_{2.96}Ti_{0.04}Sb_5$ is higher than its parent compound $CsV_3Sb_5$, which may be due to the flux pinning effect by introducing the disorders as the pinning centers.

By performing high-pressure resistivity and magnetic susceptibility measurements on Ti-doped $CsV_{3-x}Ti_xSb_5$ ($x = 0.04$ and 0.15) single crystals, the phase diagram was constructed by tracking the evolutions of CDWs and SC. There are some differences with respect to the phase diagrams of the parent $AV_3Sb_5$ ($A = $ K, Rb, or Cs) family [16,17,20,21]. For example, the superconducting dome for parent compounds under high pressure is strongly correlated with the $A$-cation radius or the interlayer distance, which changes from an M-shaped double dome to a shallow double dome and then to a single dome by reducing the $A$-site size from Cs to Rb and then to K [16,17,20,21]. While in $CsV_{2.96}Ti_{0.04}Sb_5$, the $T^*(P)$ exhibits a monotonic suppression under high pressure as with the $AV_3Sb_5$ family, the superconducting $T_c$ displays a different evolution as a function of pressure. Under high pressure, $T_c^{\text{onset}}$ shows an obvious single-dome structure centering around the QCP of the CDW. However, the first dome of $T_c^{\text{zero}}$ that was associated with the modification of the CDW at $P_{c1}$ was smeared out, leaving a plateau feature. This anomaly may correlate with a suppression of the short-range unidirectional $4a_0$ CDW by pressure or a strong disorder scattering effect. Moreover, the critical pressure $P_{c2} \sim 1.66$ GPa is lower than that $\sim$2 GPa in the parent compound $CsV_3Sb_5$, which should have a direct correlation with the CDW ordering temperature $T^*$. As is shown in Fig. 4(b), the single-dome superconducting phase peak at $\sim$1.5 GPa can be easily discerned in $CsV_{2.85}Ti_{0.15}Sb_5$, which shows no long-range CDW.

With increasing the Ti-doping level at AP, the CDW ordering temperature $T^*$ shows a decrease at $x \sim 0.04$ and then

vanishes completely at $x \sim 0.15$, while the superconducting $T_c$ first decreases with the suppression of CDW and then was enhanced again when the CDW was completely suppressed. Recently, the nonmagnetic impurity effect on the CDW and SC of $CsV_3Sb_5$ was studied, and the results show that disorders introduced by electron irradiation can suppress both CDWs and SC [30]. Under high pressure, the maximum $T_c$ shows a continuous decrease from $\sim$8 to $\sim$6.3 K, with increasing the electron irradiation level from 0 to 8.6 C/cm$^2$. This indicates that chemical disorders are detrimental to the SC. On the other hand, the increased disorders in $CsV_3Sb_5$ by irradiating will shift the CDW endpoints to a lower pressure and suppress the optimal $T_c$ at the QCP of the CDW [30]. Thus, our high-pressure results on Ti-doped $CsV_3Sb_5$ are consistent with the irradiated $CsV_3Sb_5$, i.e., the CDW endpoint moves to low pressures, and the optimal $T_c$ at the critical pressure decreases gradually from $\sim$8 to $\sim$6.3 K, with $x = 0$–0.15. Consequently, the doping of Ti in $CsV_3Sb_5$ not only introduces hole carriers that suppresses the CDW but also brings disorders that suppress SC.

As indicated by the scanning tunneling microscopy (STM) results, the long-range CDW was completely suppressed in $CsV_{2.85}Ti_{0.15}Sb_5$, leaving only a local unidirectional CDW [27]. Indeed, no signature of a CDW can be detected in $\rho(T)$ curves at ambient and high pressures. As shown in Figs. 4(d) and 4(e), however, both $\mu_0 H_{c2}(0)$ and $T_c$ of $CsV_{2.85}Ti_{0.15}Sb_5$ exhibit an obvious dome-shaped structure around $P_c \sim 1.5$ GPa, where the superconducting transition width $\Delta T_c$ experiences an obvious reduction. These observations indicate that the superconducting dome may be correlated with the suppression of the short-range CDW by pressure [16,21]. Therefore, the intertwined short-range CDW fluctuations and SC still exhibit competitions.

Finally, we want to discuss the implications of our transport data on the modification of CDWs and SC in the series of Ti-doped $CsV_{3-x}Ti_xSb_5$ ($x = 0$, 0.04, and 0.15) samples. As indicated by the high-pressure NMR and transport experiments on $CsV_3Sb_5$ [16,17,19], the transition from a triple-$Q_{2a0}$ to a stripe-type CDW is accompanied with the enhanced $\Delta T_c$, the decrease of $T_c^{\text{zero}}$, and the sharp drop of magnetoresistance. According to our results, we believe that the triple-$Q_{2a0}$–to–stripe-type transition still exists in $CsV_{2.96}Ti_{0.04}Sb_5$ between $P_{c1}$ and $P_{c2}$, based on the broadening of the superconducting transition width $\Delta T_c$ [Fig. 4(d)], the flatted superconducting $T_c^{\text{zero}}$ [Fig. 4(a)], and the abrupt decrease of magnetoresistance (Fig. S4 in the SM [29]), while for $CsV_{2.85}Ti_{0.15}Sb_5$, the long-range CDW was suppressed gradually by hole doping and disorders, and only a local CDW can be detected by STM [27]. Then the double-dome superconducting phase gradually evolves to a single dome under high pressure. On the other hand, based on the DFT calculations for $CsV_3Sb_5$ at AP and high pressures, the corresponding change of anomalies around $T^*$ in $\rho(T)$ and $d\rho/dT$, and $\Delta T_c$ around $P_{c1}$ should originate from the quench of the out-of-plane wave vector of the CDW along the $c$ axis, due to the faster compression of the $c$ than the $a$ axis and the related more dispersive band structure along the $c$ axis [16]. For $CsV_{3-x}Ti_xSb_5$, the ARPES measurements and DFT calculations demonstrate that the Fermi energy gradually shifts down with increasing the Ti-doping level, but the band dispersion only shows slight changes at AP [27]. Moreover,

the disorders induced by Ti doping at V sites will gradually weaken the phase coherence of the CDW along the $c$ axis and will pin the CDW distortions at AP. Thus, it will further affect the evolution of CDWs and SC under high pressure. Our results further demonstrated that the CDW and SC have intimate correlations in the kagome superconductor $AV_3Sb_5$ family.

In addition, $\mu_0 H_{c2}(0)$ shows the prominent maximum at $P_{c2} \sim 1.66$ GPa in $CsV_{2.96}Ti_{0.04}Sb_5$, indicating the existence of quantum criticality associated with the CDW. Our high-pressure study on the $CsV_{3-x}Ti_xSb_5$ family sheds more light on understanding the intimate competition and correlation between CDWs and SC in the kagome superconductors.

## IV. CONCLUSIONS

In summary, we have conducted a comprehensive high-pressure study on the series of Ti-doped $CsV_{3-x}Ti_xSb_5$ ($x = 0.04$ and $0.15$) single crystals by measuring resistivity and magnetic susceptibility. At AP, the CDW ordering temperature $T^* \approx 94$ K in $CsV_3Sb_5$ was gradually suppressed with increasing the Ti-doping level and vanishes completely at $x = 0.15$, whereas the superconducting transition exhibits a nonmonotonic V-shaped evolution. Under high pressure, the evolution of the CDW in $CsV_{2.96}Ti_{0.04}Sb_5$ shares high similarity with its parent compound $CsV_3Sb_5$, while both critical pressures $P_{c1}$ and $P_{c2}$ of the CDW shift to lower pressures. However, the M-shaped double superconducting dome was smeared out at $P_{c1}$ in $CsV_{2.96}Ti_{0.04}Sb_5$. For $CsV_{2.85}Ti_{0.15}Sb_5$, our results reveal a dome-shaped superconducting phase which may correlate with short-range CDW fluctuations.

[1] H. M. Guo and M. Franz, Topological insulator on the kagome lattice, Phys. Rev. B **80**, 113102 (2009).

[2] W. H. Ko, P. A. Lee, and X. G. Wen, Doped kagome system as exotic superconductor, Phys. Rev. B **79**, 214502 (2009).

[3] S. L. Yu and J. X. Li, Chiral superconducting phase and chiral spin-density-wave phase in a Hubbard model on the kagome lattice, Phys. Rev. B **85**, 144402 (2012).

[4] M. L. Kiesel, C. Platt, and R. Thomale, Unconventional Fermi Surface Instabilities in the Kagome Hubbard Model, Phys. Rev. Lett. **110**, 126405 (2013).

[5] W. S. Wang, Z. Z. Li, Y. Y. Xiang, and Q. H. Wang, Competing electronic orders on kagome lattices at van Hove filling, Phys. Rev. B **87**, 115135 (2013).

[6] B. R. Ortiz, S. M. L. Teicher, Y. Hu, J. L. Zuo, P. M. Sarte, E. C. Schueller, A. M. M. Abeykoon, M. J. Krogstad, S. Rosenkranz, R. Osborn *et al.*, $CsV_3Sb_5$: A $\mathbb{Z}_2$ Topological Kagome Metal with a Superconducting Ground State., Phys. Rev. Lett. **125**, 247002 (2020).

[7] S. Y. Yang, Y. J. Wang, B. R. Ortiz, D. F. Liu, J. Gayles, E. Derunova, R. Gonzalez-Hernandez, L. Šmejkal, Y. L. Chen, S. S. P. Parkin *et al.*, Giant, unconventional anomalous Hall effect in the metallic frustrated magnet candidate, $KV_3Sb_5$, Sci. Adv. **6**, eabb6003 (2020).

[8] X. L. Feng, K. Jiang, Z. Q. Wang, and J. P. Hu, Chiral flux phase in the kagome superconductor $AV_3Sb_5$, Sci. Bull. **66**, 1384 (2021).

[9] B. R. Ortiz, E. Kenney, P. M. Sarte, S. M. L. Teicher, R. Seshadri, M. J. Graf, and S. D. Wilson, Superconductivity in the $\mathbb{Z}_2$ Kagome metal $KV_3Sb_5$, Phys. Rev. Mater. **5**, 034801 (2021).

[10] Q. W. Yin, Z. J. Tu, C. S. Gong, Y. Fu, S. H. Yan, and H. C. Lei, Superconductivity and normal-state properties of kagome metal $RbV_3Sb_5$ single crystals, Chin. Phys. Lett. **38**, 037403 (2021).

[11] F. H. Yu, T. Wu, Z. Y. Wang, B. Lei, W. Z. Zhuo, J. J. Ying, and X. H. Chen, Concurrence of anomalous Hall effect and charge density wave in a superconducting topological kagome metal, Phys. Rev. B **104**, L041103 (2021).

[12] Y. X. Jiang, J. X. Yin, M. M. Denner, N. Shumiya, B. R. Ortiz, G. Xu, Z. Guguchia, J. Y. He, M. S. Hossain, X. X. Liu *et al.*, Unconventional chiral charge order in kagome superconductor $KV_3Sb_5$, Nat. Mater. **20**, 1353 (2021).

[13] Z. W. Liang, X. Y. Hou, W. R. Ma, F. Zhang, P. Wu, Z. Y. Zhang, F. H. Yu, J. J. Ying, K. Jiang, L. Shan *et al.*, Three-Dimensional Charge Density Wave and Surface-Dependent Vortex-Core of a Kagome Superconductor $CsV_3Sb_5$, Phys. Rev. X **11**, 031026 (2021).

[14] H. Chen, H. T. Yang, B. Hu, Z. Zhao, J. Yuan, Y. Q. Xing, G. J. Qian, Z. H. Huang, G. Li, Y. H. Ye *et al.*, Roton pair density wave in a strong-coupling kagome superconductor, Nature (London) **599**, 222 (2021).

[15] L. P. Nie, K. L. Sun, W. R. Ma, D. W. Song, L. X. Zheng, Z. W. Liang, P. Wu, F. H. Yu, J. Li, M. Shan *et al.*, Charge-density-wave-driven electronic nematicity in a kagome superconductor, Nature (London) **604**, 59 (2022).

[16] K. Y. Chen, N. N. Wang, Q. W. Yin, Y. H. Gu, K. Jiang, Z. J. Tu, C. S. Gong, Y. Uwatoko, J. P. Sun, H. C. Lei *et al.*, Double Superconducting Dome and Triple Enhancement of $T_c$ in the Kagome Superconductor $CsV_3Sb_5$ Under High Pressure, Phys. Rev. Lett. **126**, 247001 (2021).

[17] F. H. Yu, D. H. Ma, W. Z. Zhuo, S. Q. Liu, X. K. Wen, B. Lei, J. J. Ying, and X. H. Chen, Unusual competition of superconductivity and charge-density-wave state in a compressed topological kagome metal, Nat. Commun. **12**, 3645 (2021).

[18] H. X. Li, G. Fabbris, A. H. Said, J. P. Sun, Y.-X. Jiang, J. X. Yin, Y.-Y. Pai, S. Yoon, A. R. Lupini, C. S. Nelson *et al.*, Discovery of conjoined charge density waves in the kagome superconductor $CsV_3Sb_5$, Nat. Commun. **13**, 6348 (2022).

[19] L. X. Zheng, Z. M. Wu, Y. Yang, L. P. Nie, M. Shan, K. L. Sun, D. W. Song, F. H. Yu, J. Li, D. Zhao *et al.*, Emergent charge order in pressurized kagome superconductor $CsV_3Sb_5$, Nature (London) **611**, 682 (2022).

[20] F. Du, S. S. Luo, B. R. Ortiz, Y. Chen, W. Y. Duan, D. T. Zhang, X. Lu, S. D. Wilson, Y. Song, and H. Q. Yuan, Pressure-induced double superconducting domes and charge instability in the kagome metal $KV_3Sb_5$, Phys. Rev. B **103**, L220504 (2021).

[21] N. N. Wang, K. Y. Chen, Q. W. Yin, Y. N. N. Ma, B. Y. Pan, X. Yang, X. Y. Ji, S. L. Wu, P. F. Shan, S. X. Xu *et al.*, Competition between charge-density-wave and superconductivity in the kagome metal $RbV_3Sb_5$, Phys. Rev. Res. **3**, 043018 (2021).

[22] T. Qian, M. H. Christensen, C. W. Hu, A. Saha, B. M. Andersen, R. M. Fernandes, T. Birol, and N. Ni, Revealing the competition between charge density wave and superconductivity in $CsV_3Sb_5$ through uniaxial strain, Phys. Rev. B **104**, 144506 (2021).

[23] M. H. Christensen, T. Birol, B. M. Andersen, and R. M. Fernandes, Theory of the charge density wave in $AV_3Sb_5$ kagome metals, Phys. Rev. B **104**, 214513 (2021).

[24] H. LaBollita and A. S. Botana, Tuning the van Hove singularities in $AV_3Sb_5$ ($A =$ K, Rb, Cs) via pressure and doping, Phys. Rev. B **104**, 205129 (2021).

[25] Y. K. Li, Q. Li, X. W. Fan, J. J. Liu, Q. Feng, M. Liu, C. L. Wang, J.-X. Yin, J. X. Duan, X. Li *et al.*, Tuning the competition between superconductivity and charge order in the kagome superconductor $Cs(V_{1-x}Nb_x)_3Sb_5$, Phys. Rev. B **105**, L180507 (2022).

[26] Y. M. Oey, B. R. Ortiz, F. Kaboudvand, J. Frassineti, E. Garcia, R. Cong, S. Sanna, V. F. Mitrović, R. Seshadri, and S. D. Wilson, Fermi level tuning and double-dome superconductivity in the kagome metal $CsV_3Sb_{5-x}Sn_x$, Phys. Rev. Mater. **6**, L041801 (2022).

[27] H. T. Yang, Z. H. Huang, Y. H. Zhang, Z. Zhao, J. N. Shi, H. L. Luo, L. Zhao, G. J. Qian, H. X. Tan, B. Hu *et al.*, Titanium doped kagome superconductor $CsV_{3-x}Ti_xSb_5$ and two distinct phases, Sci. Bull. **67**, 2176 (2022).

[28] Y. X. Liu, Y. Wang, Y. Q. Cai, Z. Y. Hao, X. M. Ma, L. Wang, C. Liu, J. Chen, L. Zhou, J. H. Wang *et al.*, Doping evolution of superconductivity, charge order and band topology in hole-doped topological kagome superconductors $Cs(V_{1-x}Ti_x)_3Sb_5$, arXiv:2110.12651 (2021).

[29] See Supplemental Material at http://link.aps.org/supplemental/10.1103/PhysRevB.107.144502 for sample characterization and high-pressure resistivity.

[30] M. Roppongi, K. Ishihara, Y. Tanaka, K. Ogawa, K. Okada, S. Liu, K. Mukasa, Y. Mizukami, Y. Uwatoko, R. Grasset *et al.*, Bulk evidence of anisotropic *s*-wave pairing with no sign change in the kagome superconductor $CsV_3Sb_5$, Nat. Commun. **14**, 667 (2023).